Quantum Behaviors on an Excreting Black Hole

James Lindesay[*]
Computational Physics Laboratory
Howard University, Washington, D.C. 20059

Abstract

Often, geometries with horizons offer insights into the intricate relationships between general relativity and quantum physics. However, some subtle aspects of gravitating quantum systems might be difficult to ascertain using static backgrounds, since quantum mechanics incorporates dynamic measurability constraints (such as the uncertainty principle, etc.).

For this reason, the behaviors of quantum systems on a dynamic black hole background are explored in this paper. The velocities and trajectories of representative outgoing, ingoing, and stationary classical particles are calculated and contrasted, and the dynamics of simple quantum fields (both massless and massive) on the space-time are examined. Invariant densities associated with the quantum fields are exhibited on the Penrose diagram that represents the excreting black hole.

Furthermore, a generic approach for the consistent mutual gravitation of quanta in a manner that reproduces the given geometry is developed. The dynamics of the mutually gravitating quantum fields are expressed in terms of the affine parameter that describes local motions of a given quantum type on the space-time. Algebraic equations that relate the energy-momentum densities of the quantum fields to Einstein's tensor can then be developed. An example mutually gravitating system of macroscopically coherent quanta along with a core gravitating field is demonstrated. Since the approach is generic and algebraic, it can be used to represent a variety of systems with specified boundary conditions.

---

[*]e-mail address, jlslac@slac.stanford.edu

1   Introduction

There have been remarkably few direct experimental observations of the quantum behaviors of gravitating systems. Experiments by Overhauser, et.al.[1], have demonstrated that those dynamic gravitational fields local to the Earth's surface do not break the coherence of gravitating neutrons, which give interference results consistent with the principle of equivalence. Those experimental results involve both Newton's gravitational constant G_N and Planck's constant $\hbar$ in a single equation form. Such results, along with other observed phenomena, require that gravitating sub-clusters can maintain quantum coherence while having their internal dynamics influenced by dis-entangled clusters co-contributing to the local gravity. Although justifications of the redshift of gravitating photons need not make use of Planck's constant, those quanta do maintain their coherence during extended interactions with dynamic gravitational fields (e.g. the cosmic microwave background, local gravitational redshift measurements, etc.). Similarly, interacting gravitating systems continue to gravitate after dis-entanglement, which motivates a formulation that incorporates straightforward cluster decomposability within macroscopic gravitational environments.

Generally, the dis-entanglement of relativistic dynamic quantum clusters that is necessary for correspondence with classical dynamics requires that the geometric aspects of the kinematics associated with the Lorentz /Poincare transformation properties of a given cluster must be separate and distinct from the internal coherent descriptions and off-shell analytic behaviors of disparate clusters. The methods utilized in this paper incorporate the techniques developed in the establishment of cluster decomposable formulations in relativistic few particle scattering[2]. Those formulations exhibit the expected dis-entanglement of interacting quantum scattering states needed for classical correspondence properties, in spite of the kinematic complications introduced by the non-linear nature of the relativistic energy-momentum dispersion relation for massive systems. The solution requires proper cluster independence of the geometric parameters describing the kinematics between subsystems from the internal quantum dynamics associated with the description of an interacting system in terms of the boundary (i.e., only *self*-interacting) states. Cluster-decomposable relativistic scattering theory is most directly realized as follows:

- the clusters should be characterized using the channel decomposition that Faddeev[3] developed for describing cluster-decomposable unitary non-relativistic systems;

- the kinematics between external and intermediate quantum states (*off-diagonal* dynamics) should insure Lorentz frame (3-velocity) conservation rather than 3-momentum conservation. Velocity conservation has been referred to as the *point form* representation of the dynamics by Dirac[4] and others, whereas momentum conservation has been referred to as the *contact form* representation;

- the internal dynamics of the intermediate quantum states (or descriptions of the interacting state in terms of the complete basis of boundary states) for the various non-interacting clusters should be independent;

- the complex analytic extension of the dynamic invariant energy of a given cluster (the *off-shell* behavior) should only parametrically affect the kinematics of the other clusters, i.e., the internal dynamics of one cluster should not alter the energy spectrum of another.

Formulations of scattering theory with these properties have been shown to have appropriate non-relativistic behaviors[5] as well as to give the expected results from perturbative representations such as quantum electrodynamics[6].

The relevant quantum dynamics is most conveniently expressed in terms of the affine parameter associated with the gravitating particles/fields. The affine or proper time derivative of local physical parameters can be expressed in terms of the substantive derivative $\frac{d}{d\lambda} = u^\beta \frac{\partial}{\partial x^\beta} \equiv u^\beta \partial_\beta$. This then makes the incorporation of the principles of equivalence/relativity straightforward, resulting in substantive quantum flows on the geometry[7].

Macroscopic quantum fluids (e.g. superfluids and superconductors) maintain persistent quantum flows that satisfy quantization conditions in the non-inertial environments of most laboratory measurements. For instance, vortices of superflow with quantized circulation maintain the angular momentum of a rotating vessel of liquid helium cooled below the superfluid transition temperature. (It would be quite interesting to see if the precession of vortices with quantized circulation $\frac{h}{m}$ in a gravitational field G_N is a measurable phenomenon.) Fluid continuity directly follows

from the equations of motion resulting from Lagrangians constructed using substantive derivatives. Superfluid flows then result from the local gauge invariance of those Lagrangian forms. Thus, substantive flows have been quite useful in describing macroscopic behaviors of quantum fluids.

Substantive quantum flows inherently articulate the philosophical approach of proper time formulations[8] that presume the primacy of coordinates associated with the system being influenced in descriptions of the interaction. One expects that the affects of external interactions upon a given system can be most fundamentally understood in terms of the dynamical parameters of that impacted system. Thus, when combined with the principle of equivalence, the dynamics of free quantum fields in a gravitating environment can be most elegantly described using the affine (proper) parameters of that quantum field. Furthermore, formulations that exemplify cluster decomposibility and substantive affine flows are most directly realized by developing linear spinor fields consistent with those in reference [9]. The form of the gravitating quanta developed in Section 4 will involve affine flows of independent states motivated by the previous discussions.

The general incorporation of quantum mechanics into gravitating formulations requires that the descriptions be dynamic, since the relationships between temporal and kinematic parameters have inherent constraints due to the quantum measurability problem (e.g. the uncetainty principle, non-commuting measurables, etc.). Therefore, the background geometry will be taken to be that of a dynamic excreting spherically symmetric space-time with a metric form given by

$$ds^2 = -\left(1 - \frac{R_M(ct)}{r}\right)(dct)^2 + 2\sqrt{\frac{R_M(ct)}{r}}dct\ dr + dr^2 + r^2\left(d\theta^2 + sin^2\theta\ d\phi^2\right).$$
$$(1.1)$$

In this equation, $R_M(ct) \equiv 2G_N M(ct)/c^2$ is a time-dependent form of the Schwarzschild radius that will be referred to as the *radial mass scale*. For this dynamic black hole, the radial mass scale is not a light-like surface, and is not coincident with the horizon (which *is* a light-like surface). However, a traversing outgoing light-like trajectory is momentarily at rest in the radial coordinate r as the radial mass scale moves past that trajectory. The trajectory of the horizon is determined by calculating the null radially outgoing geodesic $ds^2 = 0$ that intersects the radial mass scale as the mass of the black hole vanishes. This metric was developed as a dynamic extension of the river model of (static) black holes discussed in the literature[10].

The asymptotic ($r \to \infty$) form of the metric is that of a Minkowski space-time. Therefore, the coordinates (ct, r, θ, ϕ) are the temporal, radial, and angular coordinates of an asymptotic observer.

The temporal parameter t used to describe the dynamics of the black hole metric 1.1 is not singular at the horizon. More generally, physical curvatures are non-singular[11] away from $r = 0$. The contravariant form for the Einstein tensor calculated from this metric can be expressed in terms of the excretion rate $\dot{R}_M(ct)$ and the dimensionless parameter $\zeta \equiv \frac{R_M(ct)}{r}$, taking the form

$$((G^{\mu\nu})) = \begin{pmatrix} 0 & 0 & 0 & 0 \\ 0 & -\frac{\dot{R}_M(ct)}{r^2\sqrt{\zeta}} & 0 & 0 \\ 0 & 0 & -\frac{\dot{R}_M(ct)}{4r^4\sqrt{\zeta}} & 0 \\ 0 & 0 & 0 & -csc^2(\theta)\frac{\dot{R}_M(ct)}{4r^4\sqrt{\zeta}} \end{pmatrix}. \qquad (1.2)$$

Since several components of the Einstein tensor are non-vanishing, this dynamic geometry provides an excellent laboratory for the exploration of self-consistent gravitating phenomena.

The subsequent developments will exhibit the behaviors of classical and quantum objects on the black hole background described in Eqns. 1.1 and 1.2. Section 2 will exhibit solutions to the geodesic equations for the geometry, as well as demonstrate typical trajectories of massive outgoing, ingoing, and stationary classical particles on the Penrose diagram of the space-time. The expected behaviors of classical massless particles have been confirmed in a previous paper[13]. The behavior of a spherically symmetric Klein-Gordon field will be exhibited in Section 3. The form of the Klein-Gordon field will be found to be clumsy for constructing mutually gravitating fields, so a more convenient set of cluster-decomposable scalar fields will be developed in Section 4. Finally, in Section 5 an example mutually gravitating macroscopic system of quanta is exhibited and discussed.

2 Geodesic Motion

2.1 Four velocities

Geodesic motion is at the foundation of the principle of equivalence. The geodesic equation describes the evolution of four-velocities on the geometry. In all calculations, four-velocities of both massive ($\frac{dx^\beta}{dc\tau}$) and massless ($\frac{dx^\beta}{d\lambda}$) particles will be taken to be dimensionless. The form satisfied by the radial component of four-velocities on the metric 1.1 is given by

$$u^r = -\zeta^{1/2} u^0 \pm \sqrt{(u^0)^2 - \Theta_m} \tag{2.1}$$

where $\Theta_m \equiv \begin{cases} 0 & m = 0 \\ 1 & m \neq 0 \end{cases}$. In particular, stationary massive particles satisfy $u^0 = 1, u^r = -\zeta^{1/2}$. Those four-velocities associated with geodesic motion satisfy the geodesic equations:

$$\frac{du^0}{d\lambda} = -\frac{\zeta^{1/2}}{2r}(\zeta^{1/2}u^0 + u^r)^2, \tag{2.2}$$

and

$$\frac{du^r}{d\lambda} = -\frac{\dot{R}_M}{2r\zeta^{1/2}}(u^0)^2 - \Theta_m\frac{\zeta}{2r}. \tag{2.3}$$

Away from the horizon $\zeta = \zeta_H$ or the ingoing horizon $\zeta = \zeta_I$ (which of course define the geodesic of a particular outgoing or ingoing massless particle, respectively), the four-velocities of freely gravitating particles can be reparameterized in terms of the dimensionless variable ζ in the black hole geometry. This reparameterization involves the transformation

$$\frac{d\zeta}{d\lambda} = \frac{\dot{R}_M u^0 - \zeta u^r}{r}. \tag{2.4}$$

Generally, affine derivatives can be expressed in terms of the substantive (or *flow*) derivative $\frac{d}{d\lambda} = u^\beta \partial_\beta$, which, using Eqns. 2.2 and 2.3 implies that gravitating four-velocities can be expressed as functions of the single parameter ζ, i.e. $u^\beta = u^\beta(\zeta)$.

Therefore, numerical solutions of the geodesic equations can be directly obtained as ordinary differential equations. For all numerical calculations, the (dimensionless) excretion rate will be taken to be constant

$\dot{R}_M = 0.1$. This produces an outgoing horizon dressing the singularity $r = 0$ at $\zeta_H \cong 1.177$ and an ingoing horizon of outermost communication with the singularity at $\zeta_I \cong 0.078$. Plots of the four-velocities of massless particles with asymptotic values $u^0(0) = 1$ are demonstrated in Figure 1, while plots of the four-velociti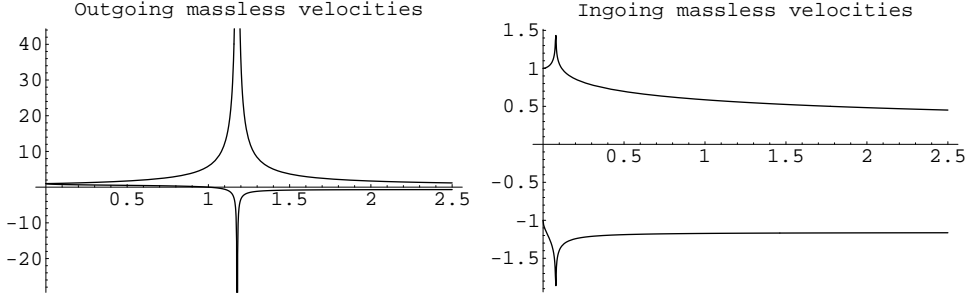es of massive particles with asymptotic values $u^0(0) = 1.2$ are demonstrated in Figure 2. The four-velocities of outgoing

Outgoing massless velocities   Ingoing massless velocities

Figure 1: Four velocities for massless particles as a function of ζ. Upper curves represent u^0 and lower u^r

Outgoing Massive Four Velocities   Ingoing   Massive Four Velocities
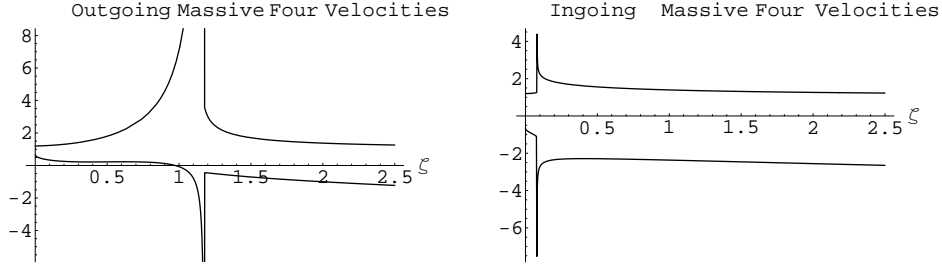
Figure 2: Four velocities for massive particles as a function of ζ. Upper curves represent u^0 and lower u^r

particles are seen to have singular behavior at the horizon $r = R_H(ct)$, while the ingoing particles have singular behavior at the ingoing horizon $r = R_I(ct)$. The radial components of the four-velocity of outgoing particles are seen to change sign at the radial mass scale $\zeta_M = 1$. Stationary massive particles are described by a vanishing value for the radical in Eqn. 2.3. The plot of stationary particles in the space-time is demonstrated in Figure 3. Any of the above-calculated forms for the four-velocities of
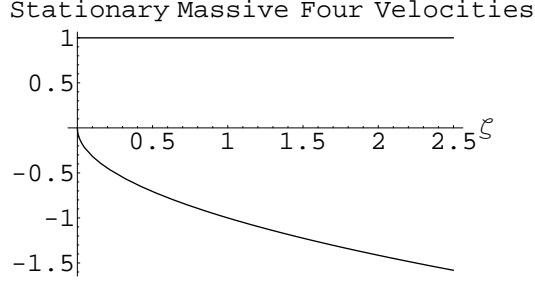
Stationary Massive Four Velocities

Figure 3: Stationary massive u^0 (upper plot) and u^r (lower plot).

massless and massive systems can then be used to develop the classical trajectories of gravitating particles.

2.2 Form of conformal coordinates

Space-time diagrams are always useful in the visualization of dynamics in a given geometry. In particular, Penrose diagrams are convenient for examining the large-scale causal structure of a geometry because of the following properties:

... Penrose diagrams map the entire space-time onto a single finite page, and

... Penrose diagrams preserve the slope of light-like trajectories at $\pm$unity.

Since light-like curves are easy to plot on a Penrose diagram, the causal structure of the geometry can be directly observed from the diagram, and potential causal relationships between locations can be immediately ascertained. In order to construct the Penrose diagram for a given space-time, conformal coordinates, which give unity slope for light-like curves, must be found. For Minkowski space-time, the coordinates (ct, r) are already conformal. However, for the metric 1.1, conformal coordinates must be constructed, since clearly null geodesics will not have unity slope for those coordinates.

For a black hole satisfying Eqn. 1.1 with a constant rate of mass accretion/excretion $\ddot{R}_M = 0$, the conformal coordinates can be determined in a straightforward manner. The forms of the conformal temporal and radial coordinates that are used for the construction of the Penrose diagram have been developed in a companion paper[12], and are given by

$$
ct_* = \frac{r}{2}\left(exp\left[\int^{\frac{R_M(ct)}{r}} \frac{\left(1+\sqrt{\zeta'}\right)d\zeta'}{\left\{\zeta'\left(1+\sqrt{\zeta'}\right)+\dot{R}_M\right\}} \right] - exp\left[\int^{\frac{R_M(ct)}{r}} \frac{\left(1-\sqrt{\zeta'}\right)d\zeta'}{\left\{\zeta'\left(1-\sqrt{\zeta'}\right)-\dot{R}_M\right\}} \right] \right)
$$

$$
r_* = \frac{r}{2}\left(exp\left[\int^{\frac{R_M(ct)}{r}} \frac{\left(1+\sqrt{\zeta'}\right)d\zeta'}{\left\{\zeta'\left(1+\sqrt{\zeta'}\right)+\dot{R}_M\right\}} \right] + exp\left[\int^{\frac{R_M(ct)}{r}} \frac{\left(1-\sqrt{\zeta'}\right)d\zeta'}{\left\{\zeta'\left(1-\sqrt{\zeta'}\right)-\dot{R}_M\right\}} \right] \right).
$$
$$(2.5)$$

This equation relates the space-time coordinates of an asymptotic observer (ct, r) with the conformal coordinates (ct_*, r_*). The Penrose diagram of a spatially coherent black hole that excretes at a constant rate $\dot{R}_M$ until it vanishes at $t = 0$, is shown in Figure 4. The singularity of the black hole is represented by the bounding space-like curve $r = 0$ on the left-hand side of the diagram. At $t = 0$, this singularity vanishes, and the curve $r = 0$ becomes time-like in the final Minkowski space-time (which is represented by the upper right quadrant of the diagram). No communication to the left of the light-like horizon R_H can escape hitting the singularity. Likewise, no communication to the right of the light-like incoming horizon R_I can communicate with the singularity. The radial mass scale $R_M(ct) = 2G_N M(ct)/c^2$ is seen to itself be a time-like trajectory where outgoing light-like trajectories remain temporarily stationary in coordinate r. The conformal coordinates (ct_*, r_*) in Eqn. 2.5 are chosen to correspond to the Minkowski coordinates (ct, r) (which are, of course, also conformal) of the asymptotic observers far from the black hole. Therefore, the bounding light-like curves on the right-hand quadrants of the diagram correspond to the Minkowski space-time of distant observers.

2.3 Classical trajectories

The classical trajectories of freely falling bodies can be directly represented on the Penrose diagram by integrating the four-velocities subject to the appropriate initial conditions. All light-like trajectories are indeed found to always have slopes of $\pm$unity[13]. Massive particle trajectories
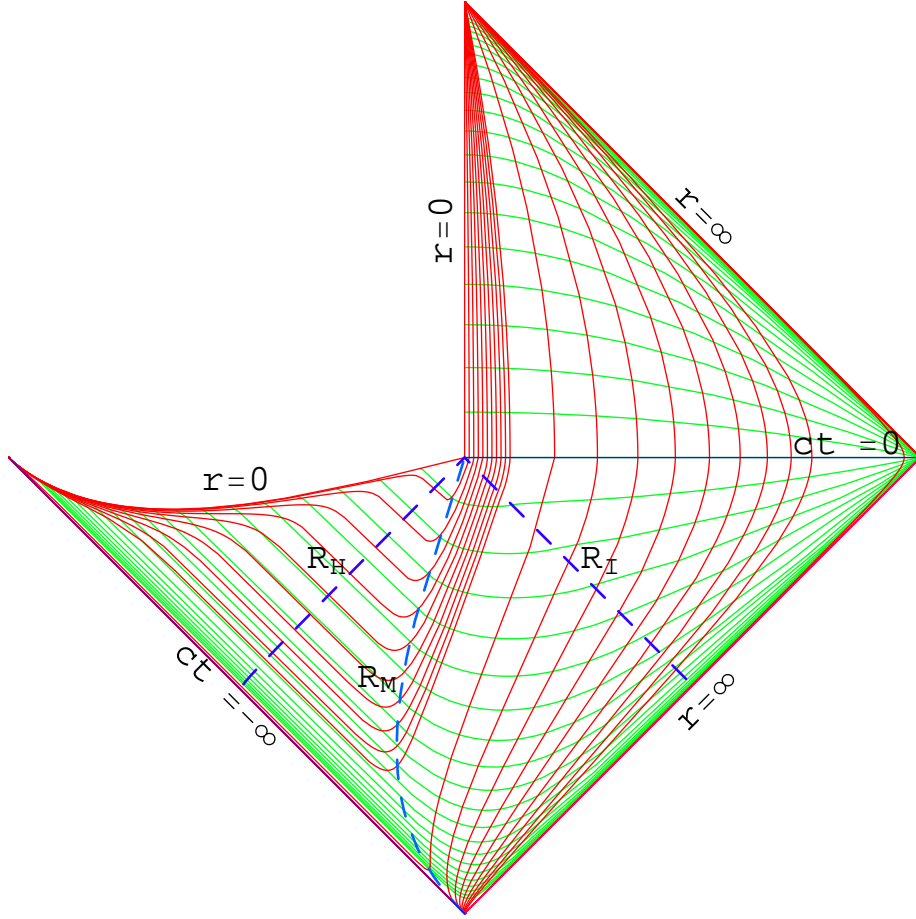
Figure 4: Penrose diagram for a black hole that evaporates steadily to zero mass at $ct = 0$. Red curves (running vertically in the right hand region) represent curves of constant r successively in tenths of units, units of length, and decades of units. The green curves represent curves of constant ct in units of length. The horizontal solid blue line on the right represents the end of excretion $ct = 0$ ($\zeta_0 = 0$), while the horizontal red curve on the left represents the space-like singularity of the black hole $r = 0$ ($\zeta_s = \infty$). The dashed blue line labeled R_H ($\zeta_H \approx 1.177$) represents the horizon, that labeled R_M ($\zeta_M = 1$) represents the radial mass scale, and that labeled R_I ($\zeta_I \approx 0.078$) represents the ingoing horizon.

are demonstrated in Figure 5. In the first diagram, various outgoing and
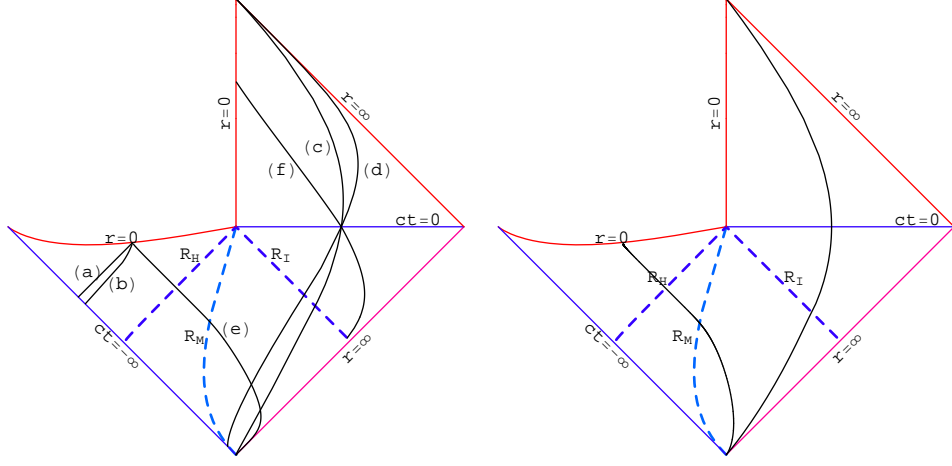

Figure 5: Classical trajectories for massive gravitating particles. The Penrose diagram on the left demonstrates outgoing trajectories (a) and (b) terminating on the singularity at $ct = -5$, outgoing trajectories (c) and (d) passing through $r = +5$ at $ct = 0$, and ingoing trajectories (e) terminating at $ct = -5$, and (f) passing through $r = +5$ at $ct = 0$. The diagram on the right demonstrates stationary trajectories terminating on the singularity at $ct = -5$, and passing through $r = +5$ at $ct = 0$.

ingoing trajectories are plotted. Trajectory (a) is an outgoing mass that ultimately hits the singularity, while trajectory (b) is an outgoing mass that hits the singularity at the same time, but moving more slowly. Trajectory (c) is an outgoing trajectory that escapes hitting the singularity, while trajectory (d) is a faster outgoing trajectory that passes through the point $(ct = 0, r = 5)$ at the same time. Trajectory (e) is an ingoing mass that hits the singularity at the same time as trajectories (a) and (b). Trajectory (f) is an ingoing mass that is external to the ingoing horizon R_I, and passes through the point $(ct = 0, r = 5)$ at the same time as trajectories (c) and (d). No numerically stable solution for massive outgoing trajectories in the region between the horizon and the radial mass scale was found. The second diagram plots the trajectories of stationary masses. The trajectory on the left of the second diagram represents a stationary mass that hits the singularity at the same time as trajectories (a), (b), and (e) on the first

diagram. The trajectory on the right of the second diagram represents a stationary mass that passes through the point $(ct = 0, r = 5)$ at the same time as trajectories (c), (d), and (f) on the first diagram. All trajectories that escape the singularity are seen to smoothly transition from gravitating projectiles to inertial free motion as the space-time transitions from dynamic black hole to Minkowski space-time at $t = 0$. It is interesting to note that a stationary particle which remains in the exterior region of the black hole geometry apparently follows the same trajectory using conformal coordinates as it would in Minkowski space-time.

3 Klein-Gordon Field

The primary focus of this paper is the examination of quantum behaviors on the dynamic space-time defined by the metric 1.1. It is instructive to first examine the quantum mechanics of a well-understood scalar field on the space-time background described by this metric. The Lagrangian of a non-interacting gravitating massless scalar Klein-Gordon field χ will take the form

$$\mathcal{L} = \frac{1}{2}\sqrt{-g}\ g^{\mu\nu}\partial_\mu\chi^*(x)\,\partial_\nu\chi(x). \tag{3.1}$$

The massless field is chosen so that no additional scale is introduced into the problem by including a mass for the quanta. As shown in reference [14], one can perform a partial wave expansion on χ

$$\chi(x) \equiv \sum_{\ell m} \frac{\psi_\ell(ct, r)}{r} Y_\ell^m(\theta, \phi) \tag{3.2}$$

to obtain equations[15] describing the dynamics of the field ψ_ℓ:

$$-\frac{\partial^2 \psi_\ell}{(\partial ct)^2} + \frac{\partial}{\partial ct}\left[\sqrt{\frac{R_M}{r}}\left(\frac{\partial \psi_\ell}{\partial r}\right)\right] + \frac{\partial}{\partial r}\left[\sqrt{\frac{R_M}{r}}\left(\frac{\partial \psi_\ell}{\partial ct}\right)\right] + \frac{\partial}{\partial r}\left[\left(1 - \frac{R_M}{r}\right)\left(\frac{\partial \psi_\ell}{\partial r}\right)\right] +$$

$$-\left[\frac{\ell(\ell+1) + \frac{R_M}{r}}{r^2} + \frac{1}{r}\frac{\partial}{\partial ct}\left(\sqrt{\frac{R_M}{r}}\right)\right]\psi_\ell = 0. \tag{3.3}$$

S-wave ($\ell = 0$) solutions of Eqn. 3.3 have been numerically calculated for the excreting black hole. Boundary conditions at $ct = 0$ require that the field ψ_0 and its derivatives must appropriately match those of a free-space

Minkowski Klein-Gordon field near that region. The matching Minkowski space solution for the field away from $r = ct$ is given by

$$\psi_M(ct, r) = \left[A + B \, log \left(\frac{r + ct}{r - ct} \right) \right] \Theta(r - ct). \qquad (3.4)$$

Plots of s-wave solutions to Eqn. 3.3 on the black hole background are shown in Figure 6. The field was chosen to have a very small (though
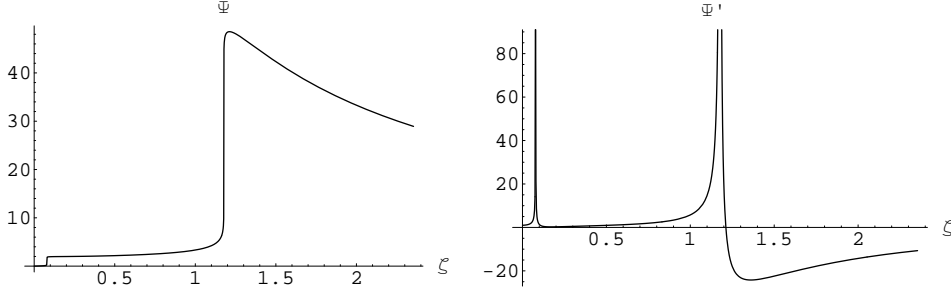

Figure 6: Plots of $\psi(\zeta)$ and $\psi'(\zeta)$ for a massless Klein-Gordon field on the dynamic black hole background, where $\zeta = R_M(ct)/r$. Field normalization units are arbitrary.

non-vanishing) value asymptotically ($\zeta = 0$). The wavefunction is continuous throughout the space-time, but its derivative is seen to have singular behavior near the ingoing horizon R_I ($\zeta_I \approx 0.078$) and the horizon R_H ($\zeta_H \approx 1.177$). The magnitude of the scalar field is seen to be largest within and near the horizon.

To gain physical insight into the distribution of the scalar field on the global space-time, a density plot on the Penrose diagram is instructive. For generating such a plot, the computer was instructed to place a pixel at a point on the Penrose diagram corresponding to the asymptotic observer's coordinate label (ct, r) if the density multiplied by a random number bounded by 0 and 1 was larger than the value calculated at a normalization point. The plot then demonstrates relative measures of the density throughout the space-time. The quantity plotted in Figure 7 is the probability density $|\chi(ct, r)|^2$. In the first density plot, the normalization point (represented by the center of the small circle) was placed on the radial mass scale curve $R_M(ct = -5)$. The second curve represents the same density, only placing the normalization point just outside of the inner
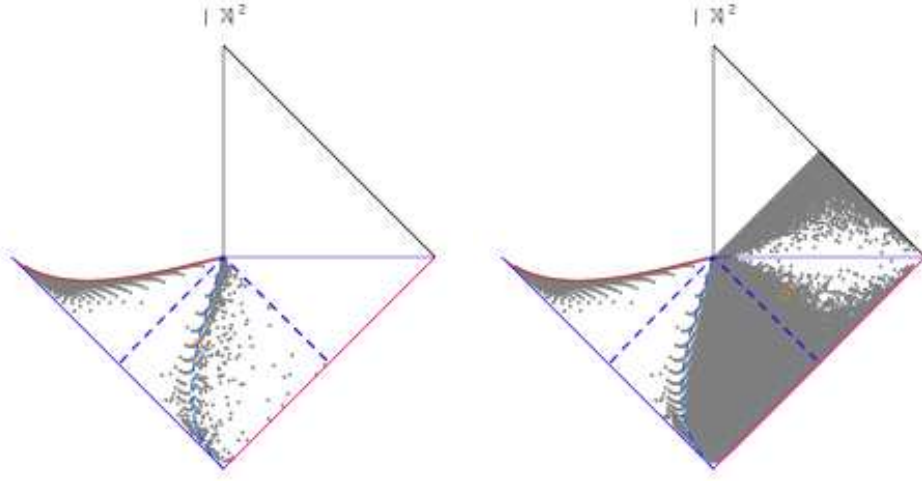
Figure 7: Penrose density plot of a spherically symmetric gravitating massless Klein Gordon field (left) and that same field's correspondence with the Minkowski space-time solution (right).

horizon, which allows smaller values of the field density to be plotted. The weak field black hole solution for the field is seen to reflect the Minkowski space-time solution that matches that field on the line (volume) $ct = 0$.

An intriguing question is whether the spherically symmetric massless Klein-Gordon field can self-gravitate to produce this black hole geometry. The energy-momentum tensor generated by the Lagrangian 3.3 can be calculated several ways. For this field, the action was calculated from the Lagrangian using $W = \int \mathcal{L} \, d^4 x$. The energy-momentum tensor was then calculated by examining the behavior of this action under variations of the metric, $\delta W \equiv \frac{1}{2} \int d^4 x \sqrt{-g} \, T^{\mu\nu} \, \delta g_{\mu\nu}$. One can then compare this tensor to the Einstein tensor 1.2 to examine how the scalar field might contribute to the gravitating system. In particular, it is convenient to examine the physical scalar density invariant $g_{\mu\nu} T^{\mu\nu}$ (i.e. the trace of the scalar field's energy-momentum tensor), which would be directly related to the Ricci scalar $\mathcal{R}$ of the space-time if the Klein-Gordon field was self-gravitating. The Klein-Gordon density invariant and the Ricci scalar are plotted in Figure 8. The density invariant is singular at the horizon and ingoing horizon, while the Ricci scalar is not. The Klein-Gordon field here calculated was not expected to directly construct a self-gravitating
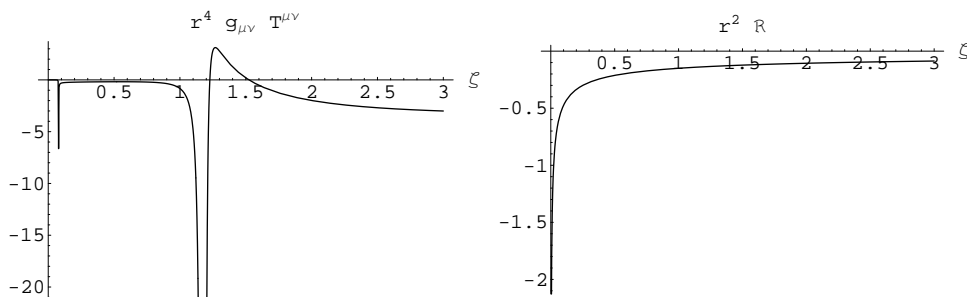
Figure 8: Plots of invariant scalar densities associated with gravitating quanta on the black hole background. The left diagram plots r^4 times the trace of the energy-momentum tensor of the Klein-Gordon field. The diagram on the right plots r^2 times the Ricci scalar of the dynamic black hole. The horizontal axis for both diagrams is the dimensionless parameter $\zeta = R_M(ct)/r$.

quantum consistent solution to Einstein's equation. The non-linear form of the Klein-Gordon energy-momentum tensor in derivatives makes superpositions clumsy. That form also makes the dependency of the density invariant upon the radial coordinate r irreparably different from that of the Ricci scalar. In addition, the form does not intuitively incorporate some of the properties that one would expect of a self-gravitating field. In the next section, a foundation will be developed for the exploration of gravitating quantum fields on a space-time background that can be superposed in a manner that might construct mutually gravitating objects.

4   Cluster-Decomposable Gravitating Scalar Fields

Useful gravitating quanta that mutually contribute to a particular space-time configuration are expected to satisfy certain physical properties:

... it should be possible to have dis-entangled components that gravitate, and can co-contribute to a mutually gravitating environment;

... the energy densities of the components should linearly contribute to the overall energy density used to drive the Einstein equation for the

gravitating environment;

... there should be components that can maintain quantum coherence, satisfying probability flux conservation and expected energy/time-momentum/position phase relationships;

... gravitating quantum systems should be able to maintain observed linearity as previously dis-entangled components interact, forming changing configurations of those systems;

... the collective gravitational field should incorporate the principle of equivalence with regards to the gravitation of a given component, i.e., one should obtain expected behaviors when performing scattering and spectroscopic experiments in a locally inertial freely falling frame.

Interacting few-particle quantum systems exhibit peculiar behaviors, such as the Efimov effect[16] (which demonstrates long range coherence for short ranged interactions), even for weakly interacting non-relativistic systems. The non-linear behavior of the energy-momentum relationship in Minkowski space-time further complicates attempts to explicitly demonstrate how interacting quantum systems can dis-entangle. The problem is that the complicated relativistic kinematics between entangled clusters will generally alter descriptions of the dynamic properties of one cluster when another cluster is interacting. For instance, in naive relativistic formulations an electron interacting on the moon would substantially affect the energy spectrum of a hydrogen atom here on earth. However, cluster-decomposable formulations of quantum scattering maintain relativistic covariance, and incorporate correspondence with the classical dis-entanglement of clusters[2, 5]. The flat space-time solution of cluster-decomposable relativistic quanta requires that one properly separate the geometry (kinematics) from the off-shell quantum dynamics. As was mentioned in the Introduction, this is done by formulating the dynamics while incorporating the following properties:

(i) a recognition of the difference between off-shell and off-diagonal descriptions of intermediate states. The off-shell behavior describes the analytic structure of the invariant energy description of the scattering amplitudes in the complex plane. Bound states manifest as poles in the off-shell parameter. The off-diagonal behavior describes

how the fully interacting system can be described in terms of a complete set of boundary states. The intermediate (virtual) state dynamics is separate from the off-energy-shell parametric behavior;

(ii) the off-diagonal description of intermediate quantum states should use Lorentz frame conservation (parameterized by preserving the three components of the four-velocity **u**, or so called *point form* dynamics) instead of momentum **p** conservation (or *contact form* dynamics);

(iii) the formulation should use parametric (geometric rather than quantum dynamic) descriptors of cluster kinematics, in terms of the invariant energies $\vec{u} \cdot \vec{P}$ for the overall system, and $\vec{u}_a \cdot \vec{P}_a$ for cluster a.

In order to most directly infuse these properties into the formulation, quantum states with explicit linear behaviors in derivatives will be constructed.

4.1 Dynamical equations of gravitating quanta

As previously mentioned, Lagrangians that utilize substantive derivatives[7] most directly incorporate the spirit of the principle of equivalence. The chosen form for the Lagrangian of a gravitating non-interacting cluster a in the geometry will be taken to be

$$\mathcal{L}_a \equiv \sqrt{-g} \ \mathrm{L}_a = -\sqrt{-g} \ [\frac{i\hbar c}{2}u^\beta(\psi_a^*\partial_\beta\psi_a - (\partial_\beta\psi_a^*)\psi_a) - m_a c^2 \psi_a^* \psi_a]. \quad (4.1)$$

Such a Lagrangian form can be directly generalized to incorporate linear spinor fields[9].

Writing the functions ψ_a as complex parameters $\psi_a \equiv |\psi_a|e^{i\xi_a}$, the Euler-Lagrange equations then insure probability conservation

$$\frac{1}{\sqrt{-g}}\partial_\beta(\sqrt{-g} \, |\psi_a|^2 u^\beta) = 0, \quad (4.2)$$

and phase coherence

$$u^\beta\partial_\beta\xi_a = -\frac{m_a c}{\hbar}. \quad (4.3)$$

Therefore, systems described by the Lagrangian form Eqn. 4.1 satisfy the dynamics expected of inertial quantum fields. Substituting the phase

coherence equation 4.3 back into the original form for the Lagrangian, it can be shown that the extremum Lagrangian for the gravitating quanta vanishes $\mathcal{L}_a = 0$.

If one defines E_m as the proper value (standard form invariant of the little group[17]) of the energy of the particle (i.e. mc^2 for massive particles, E_0 for massless particles), a general solution to Eqn. 4.3 is given by

$$\partial_0 \xi = \frac{E_m}{\hbar c}(u_0 + Q\,u^r) = \frac{E_m}{\hbar c}\left[-(1-\zeta)u^0 + (\sqrt{\zeta}+Q)u^r\right], \qquad (4.4)$$

$$\partial_r \xi = \frac{E_m}{\hbar c}(u_r - Q\,u^0) = \frac{E_m}{\hbar c}\left[(\sqrt{\zeta}-Q)u^0 + u^r\right], \qquad (4.5)$$

where the covariant forms of the 4-velocities are given by

$$u_0 = (\zeta - 1)u^0 + \zeta^{1/2}u^r,$$
$$u_r = \zeta^{1/2}u^0 + u^r. \qquad (4.6)$$

The four-velocities satisfy the usual normalization $u^\beta u_\beta = -\Theta_m$.

The integrability of a function of several variables means that the function is in fact well described in terms of those variables, satisfying the analytic property of equality of second partial derivatives regardless of order. The integrability of the phase $[\partial_r, \partial_0]\,\xi(ct,r) = 0$ implies that the function Q must satisfy

$$u^\beta \partial_\beta Q = \partial_0 u_r - \partial_r u_0 - \left(\partial_\beta u^\beta\right)Q. \qquad (4.7)$$

Since the four-velocities depend only on the the dimensionless parameter ζ, $u^\beta = u^\beta(\frac{R_M(ct)}{r})$, the functions $Q = Q(\zeta)$ can likewise be shown to depend only upon the dimensionless parameter ζ. For the metric form 1.1, derivatives of the geodesic four-velocities (from Eqns. 2.2 and 2.3) satisfy

$$\partial_\beta\,u^\beta = \frac{\Theta_m}{r}\frac{\zeta^{1/2}}{2}\frac{\dot{R}_M + \zeta^{3/2}}{\dot{R}_M u^0 - \zeta u^r}, \qquad (4.8)$$

and

$$\partial_0 u_r - \partial_r u_0 = 0. \qquad (4.9)$$

Numerical solutions for the magnitudes and phases of the fields can be developed by defining the dimensionless parameters $|\tilde{\psi}(\zeta)|^2$ by the equation

$|\psi(ct,r)|^2 \equiv \frac{|\tilde{\psi}(\zeta)|^2}{L_P\, r^2}$, and the reduced phases $\tilde{\xi}(\zeta)$ (which carry the dimension of inverse Compton wavelength) by the equation $\xi(ct,r) \equiv r\tilde{\xi}(\zeta)$. It is interesting to note that $|\tilde{\psi}(\zeta)|^2$ and $Q(\zeta)$ have the same form for their differential equations.

For massless particles, one can immediately determine that the parameters $|\tilde{\psi}(\zeta)|^2$ and $Q(\zeta)$ are constants. Analytic solutions can also be obtained for stationary particles. For stationary massive particles, the solutions take the form

$$\frac{|\tilde{\psi}_S(\zeta)|^2}{|\tilde{\psi}_S(\zeta_o)|^2} = \left(\frac{\dot{R}_M + \zeta_o^{3/2}}{\dot{R}_M + \zeta^{3/2}}\right)^{1/3} = \frac{Q_S(\zeta)}{Q_S(\zeta_o)}. \tag{4.10}$$

Numerical forms describing the quantum dynamics of outgoing and ingoing massive quanta can directly be obtained by solving the straightforward ordinary differential equations for the phase factor $Q(\zeta)$ (as well as the reduced squared wavefunction $|\tilde{\psi}(\zeta)|^2$) using Eqn. 4.7, and integrating Eqn. 4.4 to obtain the phase ξ.

4.2 Energy-momentum tensors of gravitating quanta

The form of the contribution of the gravitating quanta to the energy-momentum tensor can be directly calculated using the standard Legendre transformation from the Lagrangian form to the Hamiltonian form of the dynamics of a multi-component field χ:

$$\mathcal{T}^\beta_{\ \mu} = \sum \frac{\partial \mathcal{L}}{\partial(\partial_\beta \chi)} \partial_\mu \chi - \delta^\beta_\mu \mathcal{L}. \tag{4.11}$$

The Euler-Lagrange equations imply that the extremal form of the Lagrangian 4.1 vanishes $\mathcal{L}_a = 0$ for any quantum a. Therefore, the energy-momentum tensor of quantum a satisfies

$$\mathcal{T}^\beta_{a\ \mu} = \sqrt{-g}T^\beta_{a\ \mu} = \sqrt{-g}(\hbar c)u^\beta_a(\partial_\mu \xi_a)|\psi_a|^2. \tag{4.12}$$

The energy-momentum contribution of quantum a to the overall system is seen to depend linearly upon derivatives of the phase, directly linking the local phase of the wavefunction a to its contribution to the local energy-momentum of the system.

The form of these generic quanta need not locally conserve energy-momentum due to the background gravitation. The generic form for the

divergence of the of the energy-momentum tensor of a field ψ_a is given by

$$T^{\beta}_{a\,\mu\,;\beta} = -\Gamma^{\lambda}_{\mu\beta}\frac{\partial \mathrm{L}_a}{\partial(\partial_\beta\psi_a)}\partial_\lambda\psi_a + complex\,conjugate. \qquad (4.13)$$

Neither is the form of this tensor necessarily symmetric, satisfying

$$T^{0\,r}_a - T^{r\,0}_a = \Theta_{m_a}\frac{m_a c}{\hbar}\,|\psi_a|^2\,Q_a. \qquad (4.14)$$

Since the Einstein tensor 1.2 is both geometrically conserved and symmetric, the collective form of the energy-momentum tensor driving the Einstein equation must likewise be locally conserved and symmetric.

5   Macroscopic Self-Gravitating Quanta

Although the form of microscopic quantum gravity remains uncertain, the quantum mechanics of systems co-gravitating with macroscopic media has been phenomenologically explored by common experience as well as experiment[1]. As a complement to attempts to self-consistently describe the microscopic behaviors between mutually gravitating quanta, one should be able to gain insight into the fundamentals of gravitation by developing micro-physical behaviors that consistently reproduce an example dynamic space-time. Therefore the form of mutually gravitating coherent sub-clusters that are consistent with the metric Eqn. 1.1 will be developed in this section.

The geometrodynamics of the space-time must consistently co-mingle with the micro-physical behaviors for the construction to be viable. The Ricci scalar $\mathcal{R}$ used in the calculation of the Einstein tensor is directly related to a physical invariant given by the trace of the energy-momentum tensor $T^{\beta}{}_{\beta}$. For the space-time metric 1.1, it is given by

$$\mathcal{R} = \frac{3\dot{R}_M}{2r^2}\sqrt{\frac{r}{R_M}}, \qquad (5.1)$$

which is non-singular away from a physical singularity at the origin, and vanishes for a static radial mass scale $\dot{R}_M \to 0$ for finite radial mass scales R_M. However, one should note that although the metric Eqn. 1.1 takes

the same form as a Minkowski space-time as the radial mass scale vanishes, some physical attributes of a black hole that excretes at a steady rate become singular when $R_M \to 0$ in Eqn. 5.1. This paper is not concerned with how the excretion rate $\dot{R}_M$ turns off as the radial mass scale vanishes, which is what must occur in an actual physical process. Reasonable calculations show that one can obtain viable quantum solutions with stepwise constant rate equations for radial mass scales down to the Planck length. Therefore, gravitating quantum solutions will be examined for the constantly excreting space-time represented in the lower quadrants of the Penrose diagram in Figure 4 for times $t < 0$.

5.1 Core quantum field

The Lagrangian densities for the cluster-decomposable gravitating scalars developed in Section 4 vanishes for extremal fields. The space-time described by the metric 1.1 is spherically symmetric, so that all velocities have vanishing angular components $u^\theta = 0 = u^\phi$. This means that quanta with energy-momentum tensors of the form Eqn. 4.12 cannot contribute to the non-vanishing components of the Einstein tensor $G^\theta{}_\theta$ and $G^\phi{}_\phi$. Therefore, the vanishing of the Lagrangian densities $\mathcal{L}_a = 0$ for the non-interacting gravitating quanta, requires the addition of an interacting form for a core gravitating field in order to be consistent with Einstein's equation.

The core gravitating field is expected to relate closely to classical geometric parameters, and will be represented by real fields with a Lagrangian of the form

$$\mathcal{L}_{core} = -\sqrt{-g}\,\hbar c \left[\psi_{c+}(u^\beta \partial_\beta \psi_{c+} + \tfrac{1}{2} u^\beta \partial_\beta (log\sqrt{-g})\psi_{c+}) + \right.$$
$$\left. - \psi_{c-}(u^\beta \partial_\beta \psi_{c-} + \tfrac{1}{2} u^\beta \partial_\beta (log\sqrt{-g})\psi_{c-}) \right]. \tag{5.2}$$

The core fields $\psi_{c\pm}$ satisfy the same Euler Lagrange equations, but will have opposing signs for their energy densities. The core gravitating fields are seen to have an interaction term dependent on the local form of the metric.

For the real fields $\psi_{c\pm}$, the Euler-Lagrange equations require that

$$\sqrt{-g}\,\psi_{c\pm}\,\partial_\beta u^\beta = 0. \tag{5.3}$$

From Eqn. 4.8, one observes that *any* massless core fields will satisfy these Euler-Lagrange equations. Light-like propagation properties for the core

gravitating field are, of course, intuitively gratifying. This gives considerable flexibility in choosing forms for the core fields $\psi_{c\pm}$ that are consistent with the requirements of Einstein's equation for this geometry.

The form of the core field energy-momentum tensor is given by

$$T_{core}{}^{\beta}{}_{\mu} = -\hbar c \left[\psi_{c+} u^{\beta} \partial_{\mu} \psi_{c+} - \psi_{c-} u^{\beta} \partial_{\mu} \psi_{c-} \right] - \delta^{\beta}_{\mu} \mathcal{L}_{core}/\sqrt{-g}. \qquad (5.4)$$

Einstein's equation then requires that the physical content of the system satisfies

$$G^{\beta}{}_{\mu} = -8\pi \frac{L_P^2}{\hbar c} (T_{core}{}^{\beta}{}_{\mu} + T_{rad}{}^{\beta}{}_{\mu}) \qquad (5.5)$$

where the Planck length is defined by $L_P \equiv \frac{\hbar}{M_p c} = \sqrt{\frac{\hbar G_N}{c^3}}$ and the tensor of radiating quanta T_{rad} is the collective form of the cluster-decomposable quanta developed in Section 4. As previously stated, since the radiations defined in Eqn. 4.1 cannot contribute to $G^2{}_2 = G^3{}_3$ for a spherically symmetric system (since $u^{\theta} = 0 = u^{\phi}$ in the equation 4.12 for the radiating components' contributions), Einstein's equation constrains the form of the core gravitating field from Eqn. 1.2,

$$-\frac{\dot{R}_M}{4r^2\sqrt{\zeta}} = G^3{}_3 = -8\pi \frac{L_P^2}{\hbar c} T_{core}{}^3{}_3 = 8\pi \frac{L_P^2}{\hbar c} \mathcal{L}_{core}/\sqrt{-g}, \qquad (5.6)$$

which yields the equation satisfied by the core gravitating fields

$$\frac{\dot{R}_M}{16\pi L_P^2 r^2 \sqrt{\zeta}} = (u^{\beta}\partial_{\beta}\psi_{c+}^2 + \frac{2u^r}{r}\psi_{c+}^2) - (u^{\beta}\partial_{\beta}\psi_{c-}^2 + \frac{2u^r}{r}\psi_{c-}^2). \qquad (5.7)$$

A solution of Eqn. 5.7 with positive semi-definite probability densities can be found. The solution required (i) outgoing massless core quanta, (ii) $\psi_{c+} = 0$ for $r < R_H(ct)$ and (iii) $\psi_{c-} = 0$ for $r > R_H(ct)$. If described in terms of a single core field, the square of that single field simply changes signs across the horizon. Solutions are demonstrated for reduced core probability density $|\tilde{Y}_c(\zeta)|^2$ (where $|\psi_c(ct,r)|^2 \equiv \frac{|\tilde{Y}_c(\zeta)|^2}{L_P^2 r}$) and reduced core energy density $\frac{L_P^2 r^2}{\hbar c} T^{00}_{core}$ in Figure 9. The solution for the square of the core wavefunction is everywhere non-negative, but vanishes at the horizon $\zeta_H \cong 1.177$. The core field energy density is negative in regions distant from the black hole (for $\zeta < 0.2$), positive in the region outside but
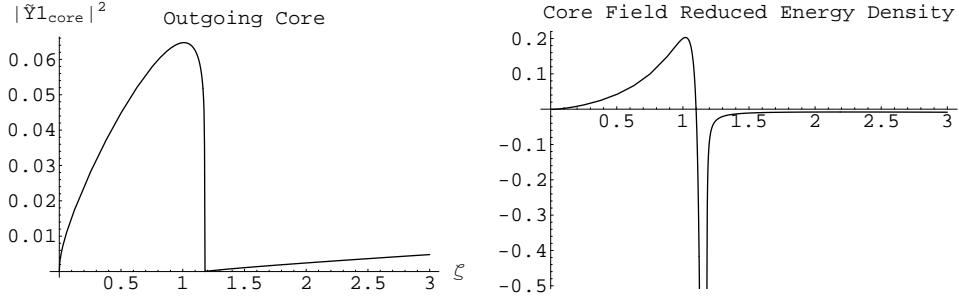
Figure 9: Reduced wavefunction squared and energy density of core field as a function of $\zeta = R_M(ct)/r$.

near the horizon ζ_H, and again negative inside the horizon. Since the component G^{00} vanishes, the sign taken by the energy density of the radiating quanta from Section 4 must cancel the energy density contributed by the core field. It was therefore crucial that the asymptotic form of the core field have this negative energy density so that normal gravitating particles far from the black hole have the expected sign for their energy densities.

As was seen for the Klein-Gordon field in Section 3 it is illustrative to examine a density plot of the physical densities calculated in Figure 9 on the global space-time represented by the Penrose diagram. As was previously discussed, only that portion of the Penrose diagram satisfying $t < 0$ will be physically populated. The square of the core field wavefunction and energy density are plotted in Figure 10. As with all density plots, these plot
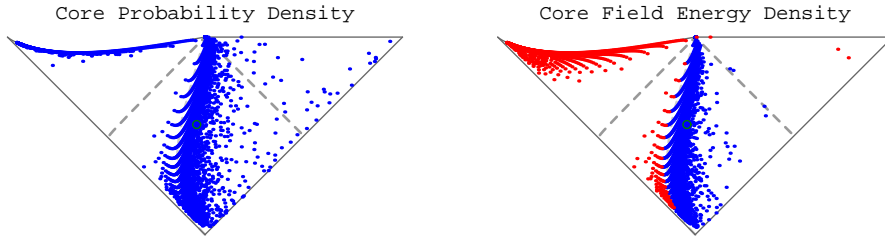

Figure 10: Penrose density plots of core field probability density and energy density.

represent the relative magnitude of the given density in terms of the relative number of pixel points plotted in a given vicinity. The normalization point

is represent by the small circle in the middle of the diagram near the radial mass scale $\zeta_M = 1$. Since the physical parameters being plotted might take on negative values, a blue pixel is plotted if the density is positive relative to the absolute value of the normalization scale, while a red pixel is plotted if it is negative relative to the negative absolute value of the normalization scale. The core field energy density is seen to take on negative values in the interior region, as well as small negative values in far regions on the right of the Penrose diagram.

Solutions of Eqn. 5.7 involving ingoing massless core quanta were likewise calculated. The solution for ingoing massless core quanta obtained by the author had negative probability densities in a small region near the radial mass scale (within numerical accuracy), and were not further explored.

5.2 A mutually-gravitating macroscopic system

Once the core gravitating field of the excreting black hole has been determined from Eqn. 5.7, the linear behavior of the radiation fields can be exploited to construct a mutually/self gravitating system. Substituting solutions for the core field calculated from Eqn. 5.7 into the core energy-momentum in Eqn. 5.4, this energy-momentum tensor then placed into Einstein's equation 5.5 defines a form that must be satisfied by the collection of radiating gravitating quanta.

From Eqn. 4.12, a generic form for the macroscopic gravitating quanta is given by

$$T_{rad}{}^{\beta}{}_{\mu} = \sum_a (\hbar c) u_a^{\beta} (\partial_\mu \xi_a) |\psi_a|^2. \tag{5.8}$$

It is very gratifying that in the exterior region of the black hole, there are many, many solutions satisfying Einstein's equation 5.5 due to the algebraic and dis-entangled nature of the contributions from the radiating quanta. This means that the phenomenologically observed behaviors of dynamic spherically symmetric stars, planets, etc. can likely be incorporated using mutually gravitating particles as described by the linearly additive Eqn. 5.8.

An example solution for a mutually gravitating macroscopically coherent system of quanta will be directly demonstrated. Since there are 4 components of the Einstein tensor Eqn. 1.2 that remain to be satisfied by Eqn.

5.5, a minimal algebraic solution should be obtained using 4 particle types in Eqn. 5.8. The geometry should have coherent emissions/absorptions of otherwise conserved radiating quanta locally contributing to the energy-momentum of the system in the form

$$T_{rad}{}^{\beta}{}_{\mu} = (\hbar c)\left[u_1^{\beta}(\partial_{\mu}\xi_1)N_1|\psi_1|^2 + u_2^{\beta}(\partial_{\mu}\xi_2)N_2|\psi_2|^2 + \right.$$

$$\left. u_3^{\beta}(\partial_{\mu}\xi_3)N_3|\psi_3|^2 + u_4^{\beta}(\partial_{\mu}\xi_4)N_4|\psi_4|^2\right],$$

(5.9)

where N_a represents the number of quanta of type a present in the gravitating system. As long as the fields are linearly independent, solutions to Einstein's equation 5.5 using macroscopic quantum fields of the form in Eqn. 5.9 can always be found. However, one is not guaranteed that physical boundary conditions with positive semi-definite number densities can be found. It was found to be quite straightforward to obtain physically meaningful solutions with positive number densities and positive mass quanta in the region exterior to the radial mass scale $r > R_M$. However, the author has yet to develop solutions that have both positive semi-definite number densities and positive semi-definite masses in all regions. This is likely due to the behavior of the component u^r as seen in Eqn. 2.3, since it can change its sign in the interior region of the black hole, and therefore affect the algebraic solutions. An example macroscopic mutually gravitating excreting black hole is given below.

The solution demonstrated in Figures 11, 12, 13, and 14 involve a system with four particle types. Particle types 1 and 2 are stationary gravitating quanta with mass m and linearly independent phases demonstrated in Fig. 11. The reduced phases $\tilde{\xi}(\zeta) \equiv \frac{\hbar}{mc}\frac{\xi(ct,r)}{r}$ of the stationary particles are represented in the first two diagrams in the figure. The magnitude squared of the reduced wavefunction of the stationary particles $|\tilde{\psi}_a(\zeta)|^2 \equiv r^2 L_P|\psi_a(ct,r)|^2$ is represented in the third diagram in the figure. The singular behavior in the stationary form of $|\tilde{\psi}(\zeta)|^2$ occurs at $\zeta_{SS} = (-\dot{R}_M)^{2/3} \cong 0.215$ for the excretion rate chosen for this paper, which is in the region of the space-time between the radial mass scale R_M ($\zeta_M = 1$) and the ingoing horizon R_I ($\zeta_I \cong 0.078$). In Figure 12 particle type 3 is an outgoing massless quantum represented by the first diagram and particle type 4 is an ingoing massless quantum represented by the second diagram. The reduced wavefunction for massless quanta is constant,
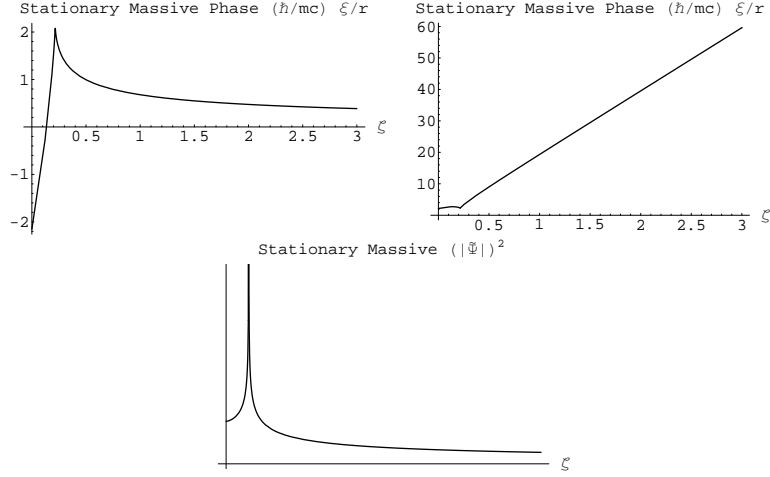
Figure 11: *Phases of stationary mass 1 and mass 2, and the square of the reduced stationary wavefunction.*
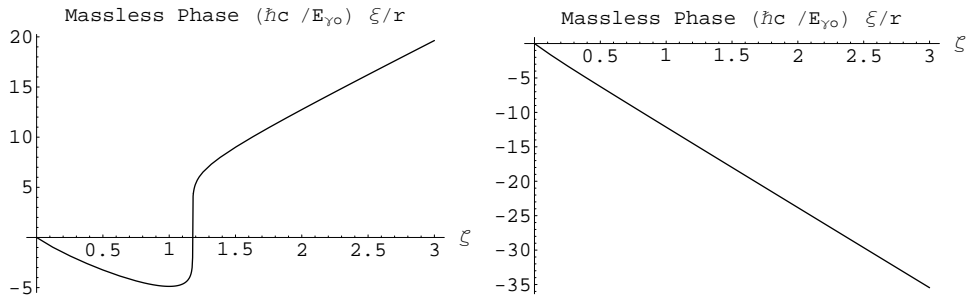

Figure 12: Outgoing and ingoing massless particle phases.

and the reduced phase is expressed in terms of the quantum's asymptotic energy E_o using $\tilde{\xi}(\zeta) \equiv \frac{\hbar c}{E_o}\frac{\xi(ct,r)}{r}$.

Algebraic solutions for the reduced number densities of the four particle types $\mathcal{N}_a(\zeta) \equiv \frac{E_{m_a}}{\hbar c}L_P^2\, r^2\, N_a(ct,r)|\psi_a(ct,r)|^2$ (where again E_m is the *proper* or *affine* energy form of a quantum of mass m), are demonstrated in Figure 13. The plot representing a particular particle type is directly
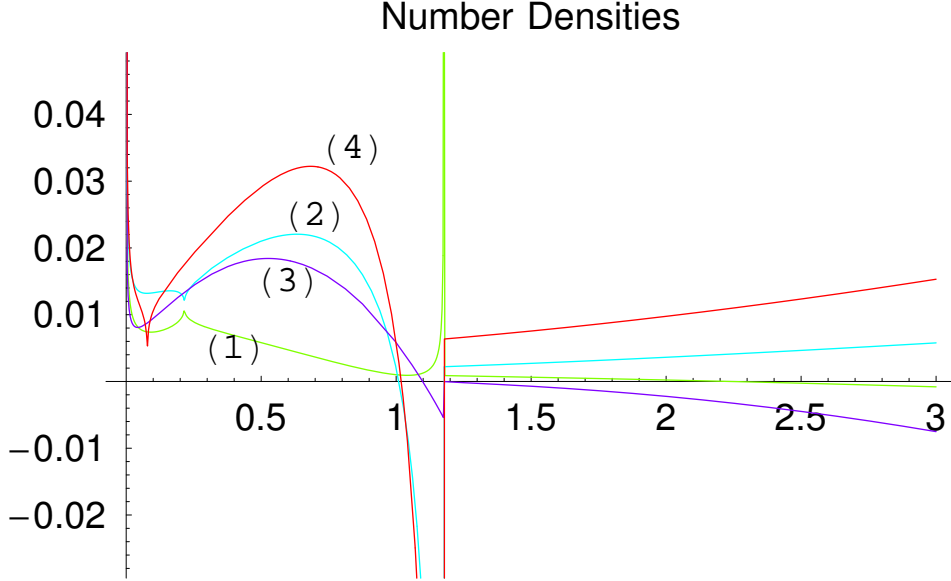

Figure 13: Reduced number densities of mutually gravitating quanta. Particle types (1) and (2) are stationary massive quanta. Particle type (3) is an outgoing massless quantum, while particle type (4) is an ingoing massless quantum. The horizontal axis is the dimensionless scale $\zeta = R_M(ct)/r$

labeled on the diagram. The affine energy form E_{m_a} (associated with the affine parameter describing the particle motion) appears in the phase of the wavefunction of particle type a as is the case with standard quantum mechanics. For massive states it represents the "co-moving" energy mc^2, while for massless states is represents the "standard state" energy-momentum E_0 of the particle observed in the boundary inertial reference frame. One can see that particle types 2, 3, and 4 must take on negative values of E_m in the region just inside of the radial mass scale $r = R_M(ct)$ ($\zeta_M = 1$), and

outside of the horizon $r = R_H(ct)$ $(\zeta_H \sim 1.2)$, if the quantum number densities of those particle types are to remain positive semi-definite. Thus, one expects to find some negative mass stationary quanta of type 2 just inside the radial mass scale, but outside of the horizon. Particle type 1 is seen to require a negative mass value inside the horizon near the singularity. Since the solutions to Eqn. 5.5 are algebraic and only depend upon Einstein's equation, the number densities themselves are independent of the normalization of the wavefunctions. Only the actual numbers of quanta satisfying a particular flux normalization depend upon the form of that normalization. Since the problem examined here has unbounded past temporal extent, normalization properties will be examined using models for a complete finite duration life-cycle (accretion, then evaporation) of a black hole in subsequent papers.

It is particularly illustrative to examine density plots of the various number densities on the Penrose diagram. Density plots of the square of the wavefunction and number density of particle type 1 are displayed in Figure 14. The density plots show densities relative to a normalization
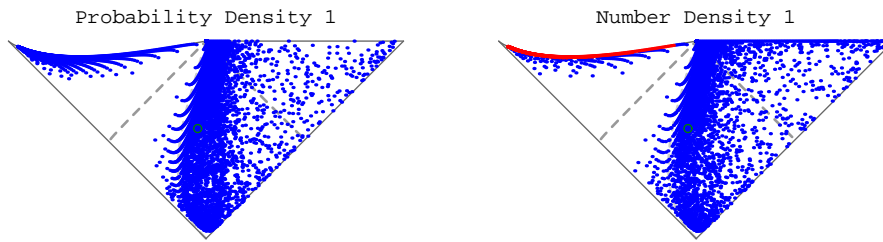

Figure 14: Penrose density plots of probability density and number density $\times$ mass of stationary mass 1

point in the center of the diagram just outside of the horizon indicated by the small circle. Once again, blue pixels indicate positive values of that density, while red pixels indicate negative values. All probability densities are found to be positive semi-definite throughout the global space-time. One might note that as previously stated, a positive semi-definite number density requires negative mass solutions near the singularity, indicated by the red values on the second density plot.

Scenarios involving various combinations of ingoing, outgoing, and stationary massive quanta co-gravitating with ingoing and outgoing massless

quanta have been calculated. The form of the four-velocities for the given geometry are fixed by the particle type (e.g. massless vs. massive). The algebraic nature of the quantum solutions make the numerical calculations straightforward. To obtain a given solution, one needs to adjust boundary values for the phases and velocities in order to match the given physical boundary conditions. It is expected that one should be able to describe physically mixed solutions (e.g. thermal systems or incoherent sums of solutions consistent with the boundary conditions) in a direct manner using this formulation.

6   Conclusions

The behaviors of classical particles and simple quantum fields on a dynamic black hole have been both analytically and numerically examined. The metric form taken to describe the dynamic black hole directly corresponds with a Minkowski space-time asymptotically, and utilizes the asymptotic observer's time coordinate to describe the dynamics of the black hole without introducing physically singular behavior at the horizon. This metric then defines the form for outgoing, ingoing, and in the case of massive particles, stationary four-velocities. These four-velocity forms are then universally applicable on the given geometry (principle of equivalence), and can be used to properly incorporate geometrodynamics (kinematics) without additional entanglements being introduced to any (internal) quantum dynamics. The trajectories of classical particles were plotted and found to satisfy the constraints expected from causality on the Penrose diagram.

In addition, simple quantum behaviors on the black hole background were seen to follow intuitively consistent behaviors. First, the form of the equation describing the dynamics of spherically symmetric solutions to the massless Klein-Gordon equation were developed. Numerical solutions of gravitating quanta on the black hole background were found to have densities most prevalent in the regions near the singularity and horizon. The numerically explored Klein-Gordon wavefunction was continuous throughout the global space-time, but its derivative was found to behave in a singular manner near the horizon and the ingoing horizon. The behavior of the energy-momentum density of the scalar field was then compared with that necessary to generate the dynamic black hole. It was found that the non-linear dependency of the Klein-Gordon energy-momentum tensor

on field derivatives make it problematic for this scalar field to be used to consistently mimic the radial dependency of the Einstein tensor describing the dynamic black hole.

Next, generic complex scalar fields whose phase relationships are linearly related to energy-momentum densities were developed. This means that the energy-momentum relationships that generate coherent phase interference properties (as experimentally observed) directly relate to the energy-momentum tensor calculated for that field. The generic form can be generalized to spinor fields in a straightforward manner. The scalar form was shown to satisfy the expected physical dynamics of quantum objects (e.g. probability flux conservation, phase coherence, etc.) on the black hole background. Numerical solutions for the quantum state vector describing the scalar fields depend only upon the boundary conditions of any given quantum state, and are straightforward to calculate. The regions of the global space time available for outgoing quanta are delineated by the black hole horizon, while regions available for ingoing quanta are delineated by the ingoing horizon of the black hole. The energy-momentum tensors of any of these quantum states linearly contribute to the overall system kinematics and dynamics.

The construction of mutual/self gravitating macroscopic collections of the scalar fields was next explored. A straightforward development of co-gravitating solutions was expected to require the following properties: (i) cluster decomposability of non-interacting radiations/quanta, (ii) proper time/affine dynamics for substantive kinematic flows in order to incorporate the principles of relativity/equivalence, and (iii) linear forms for additivity of the energy-momentum contributions. The solutions found involved the collective contributions of the energy-momentum densities of the mutually gravitating quanta combined with a real, spatially coherent *core* gravitating field resulting in a self-consistent gravitating system. The real core field for the excreting black hole examined consists of outgoing massless quanta which have a direct interaction term with the metric form in the core Lagrangian. Because of the direct metric interaction, the core fields do not have conserved probability densities, but have a form which is fixed by that of the Einstein tensor. The key points of flexibility that allows generic solutions are that the Euler-Lagrange equations for the core gravitating field only require that the field be massless, while the co-gravitating decomposable fields contribute to the overall energy-momentum densities

in an additive way directly related to the quantum phase coherence energetics.

Since the approach here taken is generic and not peculiar to the black hole examined, it should be capable of describing several physically relevant gravitational scenarios. In particular, this generic form should be useful for developing mutually gravitating solutions for static backgrounds in the exterior region (e.g. planets, stars, etc.) using ingoing and outgoing quantum stationary states, along with any kinematically stationary solutions. Fields (such as the generic gravitating quanta or gravitating clusters) with vanishing extremal Lagrangian can always be algebraically added to static geometries to help generate vacuum solutions to Einstein's equation.

The author is involved with several related on-going explorations of the geometrodynamics of gravitating quanta. One might gain insight into the microscopic contributions of the individual quantum clusters by more closely examining the single quantum limiting forms of the macroscopic system (whether the system has a singularity or not). In addition, the exploration of the co-gravitating initiation of accretion to form a singularity might answer fundamental questions on how black holes start the process of collapse. Finally, the construction of mutually gravitating cosmological systems can be likewise accomplished in a straightforward manner, as will be presented shortly in a follow up paper.

Acknowledgments

References

[1] R. Colella, A.W. Overhauser, and S.A. Werner, "Observation of Gravitationally Induces Quantum Interference", Phys.Rev.Lett. **34**, 1472-1474 (1975). See also A.W.Overhauser and R.Colella, Phys.Rev.Lett. **33**, 1237 (1974).

[2] "Self-Consistent, Poincare-Invariant and Unitary 3-Particle Theory", J. Lindesay, A. Markevich, H.P. Noyes, and G. Pastrana. Phys. Rev. **D 33**, 2339-2349 (1986).

[3] **Mathematical Aspects of the Three-Body Problem in Quantum Scattering Theory**, L. D. Faddeev, (Davey, New York, 1965).

[4] P.A.M. Dirac, Rev. Mod. Phys. **21**, 392 (1949). See also H. Leutwyler and J. Stern, Ann. Phys. **112**, 94 (1978)

[5] "A Non-Perturbative, Finite Particle Number Approach to Relativistic Scattering Theory", M.Alfred, P.Kwizera, J. Lindesay, and H.P.Noyes, hep-th/0105241, Foundations of Physics **34**(4), 581-616 (2004).

[6] "Construction of Non-Perturbative, Unitary Particle-Antiparticle Amplitudes for Finite Particle Number Scattering Formalisms", J. Lindesay and H.P.Noyes, Found. Phys. **35**(5), 39 pages (May 2005), DOI 10.1007/s10701-005-4563-8. SLAC-PUB-9156, nucl-th/0203042, 47 pages (2002).

[7] "The Geometry of Quantum Flow", J. Lindesay and H. Morrison. **Mathematical Analysis of Physical Systems**, pp 135-167, ed. by R. Mickens. Van Nostrand Reinhold, Co., New York (1985)

[8] "Canonical Proper Time Formulation for Physical Systems", J. Lindesay and T. Gill, Foundations of Physics **34**(1), 169-182 (2004). See also "Canonical Proper Time Formulation of Relativistic Particle Dynamics", T. Gill and J. Lindesay, International Journal of Theoretical Physics **32**, 2087-2098 (1993).

[9] "Linear Spinor Field Equations for Arbitrary Spins", J. Lindesay, math-ph/0308003, 9 pages (2003).

[10] "The river model of black holes", A.J.S. Hamilton and J.P. Lisle, gr-qc/0411060 (2004) 14 pages.

[11] "Coordinates with non-singular curvature for a time-dependent black hole horizon", J. Lindesay, gr-qc/0609019 (2006), *Foundations of Physics* online DOI 10.1007/s10701-007-9146-4, 15 May 2007, 16 pages,.

[12] "Construction of a Penrose Diagram for a Spatially Coherent Evaporating Black Hole", B. A. Brown and J. Lindesay, arXiv:0710.2032v1 [gr-qc] (2007) 12 pages. Class. Quantum Grav. **25** (2008) 105026 (8pp) doi:10.1088/0264-9381/25/10/105026.

[13] "Radial Photon Trajectories Near an Evaporating Black Hole Horizon," B. A. Brown and J. Lindesay, arXiv:0802.1660v1 [gr-qc] (2008) 9 pages.

[14] **An Introduction to Black Holes, Information, and the String Theory Revolution: The Holographic Universe**, L. Susskind and J. Lindesay. World Scientific, Singapore (Jan 2005), ISBN 981-256-083-1 hardback, ISBN 981-256-131-5 paperback.

[15] "An Exploration of the Physics of Spherically Symmetric Dynamic Horizons", J. Lindesay Invited talk presented at the Joint Annual Conference of the National Society of Black Physicists and National Society of Hispanic Physicists (20-24 February 2008), Washington, DC, 22 February 2008, arXiv:0803.3018 [gr-qc] 25 pages.

[16] V. Efimov, Phys. Let. **33B**, 563 (1970). Also, V. Efimov, Nucl. Phys. **A210**, 157 (1973). For experimental evidence see Hanns-Chistoph Nageri, Nature **440**, 315 (2006)

[17] **The Quantum Theory of Fields**, S. Weinberg, Cambridge University Press, New York (1995) p. 66, ISBN 0-521-55001-7.